EGG-TMI-7757

TMI-2 UPPER-CORE PARTICLE BED THERMAL BEHAVIOR

P. Kuan

Published August 1987

EG&G Idaho, Inc.
Idaho Falls, Idaho 83415

Prepared for the
U.S. Department of Energy
Idaho Operations Office
Under DOE Contract No. DE-AC07-76ID01570

ABSTRACT

Models of dryout heat fluxes of particle beds believed to be applicable to the TMI-2 upper-core particle bed are reviewed and developed. A simplified Lipinski model and a model based on flooding are shown to agree between themselves and with experiments. These models are applied to the calculation of the dryout heat flux of the TMI-2 upper-core particle bed. The TMI-2 upper-core particle bed is shown to be: (a) coolable, if little heat is transferred to it from the consolidated region below, (b) only marginally coolable, if not uncoolable, before material relocation from the consolidated region, if most of the heat in the consolidated region is transferred to it, and (c) coolable, after the relocation, regardless of heat transfer from the remaining consolidated region. Based on an analogy to quenching experiments, which show that the heat flux during the quench of a particle bed is approximately equal to the dryout heat flux, the time required to quench the TMI-2 upper-core particle bed from 2000 K to the saturation temperature of water during the accident is estimated. The bed was either quenched by 225 min after the initiation of the accident (assuming no heat was transferred to it from the consolidated region) or, at the latest, by 245 min (20 min after molten material relocation to the lower plenum from the consolidated region; assuming most of the heat generated in the consolidated region, both before and after the relocation, was transferred to the particle bed).

CONTENTS

FIGURES

TABLES

TMI-2 UPPER-CORE PARTICLE BED THERMAL BEHAVIOR

1. INTRODUCTION

From the examination work performed over the past several years, the damaged TMI-2 reactor core can be classified into four distinct regions.[1] These are: (1) a cavity at the top of the core formed by fuel collapse, (2) an upper-core particle bed of shattered fuel below the cavity, (3) a consolidated region of solidified molten fuel below the particle bed, and (4) fuel rod stubs below the consolidated region and standing fuel assemblies around the periphery of the core. In addition to core debris, particles from less than a millimeter to tens of centimeters (apparently solidified from molten fuel) were found in the lower plenum. The end-state configuration within the reactor vessel resulting from the March 28, 1979 accident is shown in Fig. 1.

A detailed account of the formation of the damaged regions is given in Ref. 1. The damage sequence is postulated as follows. Most of the coolant in the primary system was lost through the stuck-open pilot-operated relief valve on top of the pressurizer during the first 100 min of the accident. Coolant boildown in the core and initial core heatup began at about 110 min. In the next hour, the core went through a phase of heatup to about 1600 K by decay heat, then the rapid oxidation of the zircaloy cladding, and partial liquefaction of the fuel by molten zircaloy in the upper part of the core. The liquefied cladding and fuel flowed down between the fuel rods, solidified in the cooler regions of the core, and formed the lower crust of the consolidated region. When coolant was pumped through the core by the 2-B primary coolant pump at 174 min, rapid steam generation may have shattered the fuel-rod remnants in the upper part of the core to form the upper-core particle bed. Shortly after 174 min, most of the coolant in the reactor core again boiled off. At 200 min, emergency core cooling water was introduced into the primary system and it is believed that the core was filled with coolant at around 207 min. At 225 min, molten core material suddenly flowed to the lower plenum and formed the debris in that region.

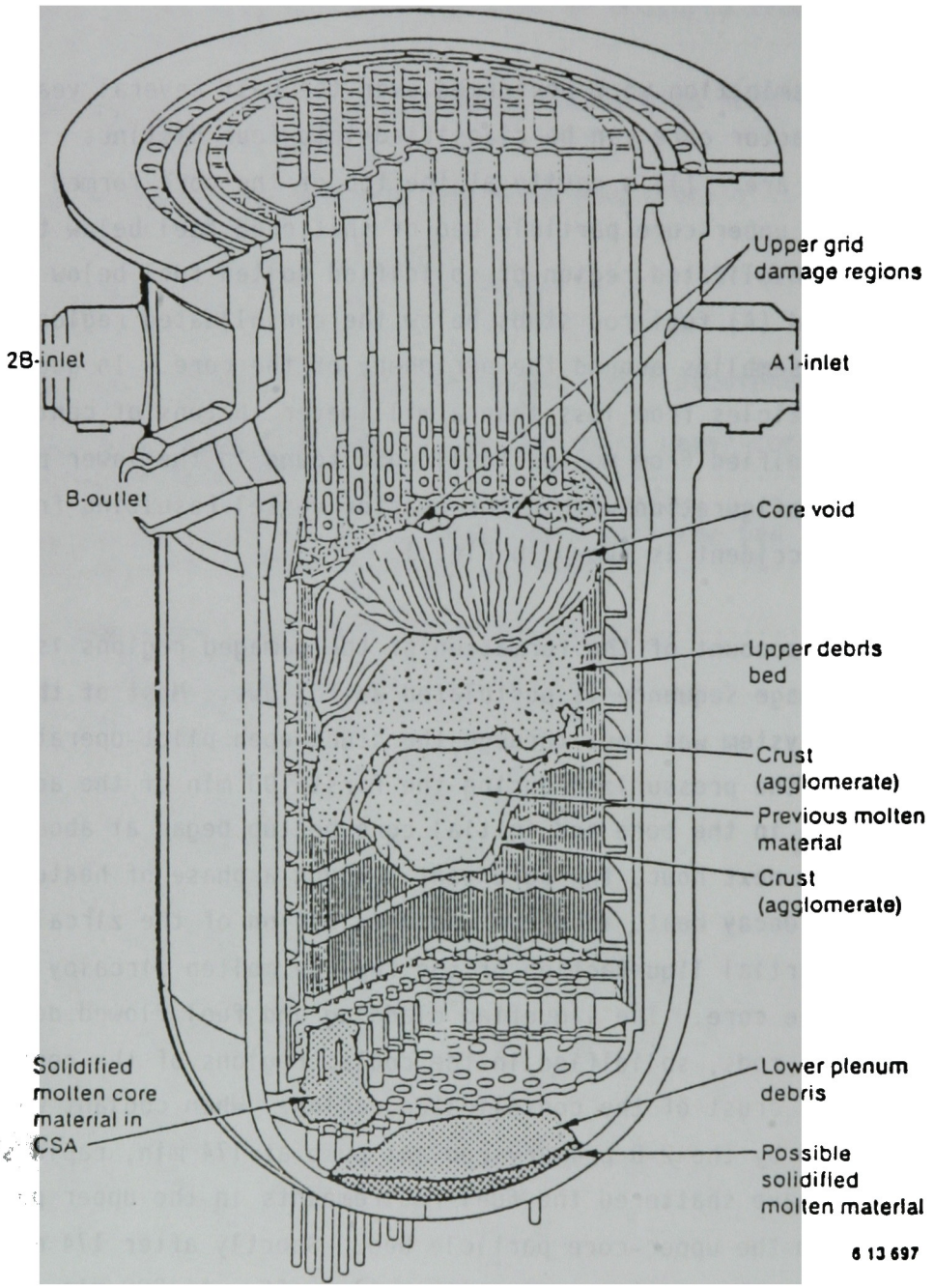

Figure 1. TMI-2 known end-state configuration inside the reactor vessel.

A one-dimensional heatup calculation, based on heat conduction in the consolidated region and a dry particle bed on top of it, showed that much of the interior of the consolidated region could have reached the melting temperature by 225 min.[2] The initiation of molten material flow to the lower plenum is not understood, although a melt-through, or mechanical failure, of the crust enclosing the molten material may have been the cause.[3]

In the transient heatup calculation, it was assumed that the upper-core particle bed was dry, even after the core was believed to have been covered with water at 207 min. The purpose of this study is to analyze the detailed thermal behavior of the upper-core particle bed regarding its dryout in the presence of water and to establish the time required to quench it from high temperatures when the core was covered with water.

Section 2 evaluates models of the dryout heat flux in heat-generating particle beds and calculates the dryout heat flux of the TMI-2 upper-core particle bed. Section 3 reviews experiments on particle bed quenching from high temperatures. Some of the experiments show that the quench heat flux is comparable to the dryout heat flux. Based on this observation, the time required to quench the TMI-2 particle bed is estimated. Section 4 presents a scenario of the thermal behavior of the TMI-2 upper-core particle bed. Uncertainties in the scenario and conclusions are given in Section 5.

2. PARTICLE BED DRYOUT

A one-dimensional particle bed, in the context of its thermal behavior, is generally characterized by the diameter of the particles composing the bed, its porosity (fractional free volume not occupied by the particles), its depth, and the volumetric heat generation rate in the bed. If the bed is immersed in a pool of liquid and has sufficient heat-generating power, the liquid in the bed boils to form vapor which flows into the overlying pool of liquid and condenses. The boiled-off liquid is replenished from the overlying pool. For a wide range of bed power, stable countercurrent flow of liquid and vapor is possible and the bed temperature is kept near the boiling point of the liquid. As the bed power is increased, a limit is finally reached when there is so much vapor generation that the liquid in the bed is completely driven out and no liquid can enter the bed from above. This condition is characterized by a critical heat flux at the top of the bed, referred to as the dryout heat flux. Once deprived of liquid, because of the much less efficient processes of heat removal by conduction and vapor convection, the interior of the particle bed will heat up rapidly to high temperatures.

Two types of models derived from apparently unrelated principles are quite successful in predicting the trend of the dryout heat flux in particle beds. One is based on pressure equilibrium between the vapor and liquid phases in the bed, as in the work of Lipinski.[4,5] In the simplified version of the model, termed 0-D, the dryout heat flux is obtained by maximizing the heat flux through the bed with respect to liquid saturation (volumetric liquid fraction in the void between the particles) under the constraints of pressure equilibrium and mass conservation. The other type of models is based on an empirical correlation for the flooding phenomena observed in packed columns used in the chemical industry. In such flooding experiments, liquid flows down and gas flows up through the bed. For a constant gas flow, there is a certain limit to the liquid flow above which the liquid is violently expelled from the bed by the gas. Similarly, with constant liquid flow, there is a limit to the gas flow above which liquid is prevented from entering the bed. These limits are termed the flooding points.[6] A series of such points constitutes the

flooding line. Sowa, et al.[7] are believed to be the first to equate the dryout heat flux as that heat flux that produces an equal amount of vapor upflow as the liquid downflow along the flooding line.

The TMI-2 upper-core particle bed consists of particles averaging 1 mm in diameter and is about 1 m thick. (The detailed characteristics of the bed is given in Section 2.4.) For such beds, it can be shown that capillary forces are relatively unimportant and the dryout heat flux is essentially independent of the bed depth. Consequently, some of the dryout models of particle beds presented below are simplified versions of their more complicated, and more general counterparts, and are specifically tailored to the application to the TMI-2 upper-core particle bed.

In Section 2.1, the Lipinski 0-D model[5] is presented. In Section 2.2, the flooding data are reexamined and used to develop a dryout heat flux correlation that is believed to have a wider range of applicability. Section 2.3 compares the 0-D and the flooding model predictions with experimental data. A best-estimate dryout heat flux for the TMI-2 upper-core particle bed is given in Section 2.4.

2.1 The Lipinski 0-D Model

To illustrate the basic concepts, the Lipinski 0-D model[5] (large particles and deep beds) for the dryout heat flux will be presented in three steps. In the process, it is hoped that the reader will gain an understanding of its applicability to the TMI-2 upper-core particle bed and some of the uncertainties associated with the model. The laminar flow regime is first considered, followed by the turbulent limit regime, and then the transition regime from laminar to turbulent flow.

2.1.1 Laminar Flow

Consider a particle bed composed of uniform, spherical particles of diameter d, having a porosity ϵ. Analogous to flow in a pipe, the hydraulic diameter, D_H, of the particle bed may be defined as

$$D_H = 4\,V_f/P \quad , \tag{2-1}$$

where

V_f = bed fluid volume, and

P = surface area of particles in bed.

In terms of the particle diameter, d, and the porosity, ε,

$$D_H = (2/3)\,\varepsilon d/(1 - \varepsilon) \quad . \tag{2-2}$$

A Reynolds number, Re, to be consistent with later references to it in this study, may be defined as

$$Re = \left(\frac{3}{2}\right)\rho v' D_H/\mu \quad , \tag{2-3}$$

where

v' = true fluid velocity,

ρ = fluid density, and

μ = fluid dynamic viscosity.

If the void space in the particle bed can be considered as a series of parallel channels, the true velocity v' is related to the superficial velocity v_o (the fluid velocity in the absence of the particles) by

$$v' = v_o/\varepsilon \quad . \tag{2-4}$$

In laminar flow through a pipe, the pressure drop per unit length of pipe is given by

$$\Delta p/L = \frac{64}{Re} \cdot \frac{1}{2} \rho v'^2 \cdot \frac{1}{D_H} \qquad (2\text{-}5)$$

where

Δp = pressure drop, and

L = length of pipe.

If this analogy is carried to a particle bed, Eq. (2-5) gives

$$\Delta p/L = \frac{48\ \mu v_o\ (1 - \epsilon)^2}{\epsilon^3 d^2} \quad . \qquad (2\text{-}6)$$

where L is now the height of the particle bed.

Because of the tortuous fluid path through a particle bed, the measured pressure drop through the bed is in fact higher than that given by Eq. (2-6).[8] A good fit to the experimental data is to replace the numerical coefficient 48 by 150, i.e.,

$$\Delta p/L = \frac{150\ \mu v_o\ (1 - \epsilon)^2}{\epsilon^3 d^2} \quad . \qquad (2\text{-}7)$$

which is the Blake-Kozeny equation for pressure drop through a particle bed.[8] Equation (2-7) is generally valid for porosities less than about 0.5 and for Reynolds numbers, as defined by Eq. (2-3), less than about 5. In the region of its validity, experimental values of the pressure drop differ from those given by Eq. (2-7) by only a few percent.

For two-phase flow through a particle bed, because of flow area reduction for each phase and because of the friction between the phases,

the pressure drop for each phase is enhanced from the value given by Eq. (2-7). Lipinski[5] used the functions developed by Cory from experimental data to obtain

$$\Delta p_g/L = \frac{150\ \mu_g v_g\ (1 - \varepsilon)^2}{\varepsilon^3 d^2\ (1 - s)^3} \quad , \text{ and} \tag{2-8}$$

$$\Delta p_\ell/L = \frac{150\ \mu_\ell v_\ell\ (1 - \varepsilon)^2}{\varepsilon^3 d^2 s^3} \quad , \tag{2-9}$$

where the subscripts g and ℓ denote vapor and liquid, respectively, and the velocities are the superficial velocities of the phases. (Note that v_ℓ is considered positive in the downward direction). The symbol, s, denotes an effective liquid saturation given by

$$s = \frac{s_t - s_r}{1 - s_r} \quad , \tag{2-10}$$

where s_t is the true saturation, and s_r a residual saturation somewhere near 0.17.[5] (The true saturation is defined as the volumetric liquid fraction occupying the void space between the particles.)

If both phases are continuous in the particle bed (separated flow), adding the hydrostatic terms to Eqs. (2-8) and (2-9) gives

$$\Delta p_g/L = \rho_g g + \frac{150\ \mu_g v_g\ (1 - \varepsilon)^2}{\varepsilon^3 d^2\ (1 - s)^3} \quad , \text{ and} \tag{2-11}$$

$$\Delta p_\ell/L = \rho_\ell g - \frac{150\ \mu_\ell v_\ell\ (1 - \varepsilon)^2}{\varepsilon^3 d^2 s^3} \quad , \tag{2-12}$$

where

ρ_g = vapor density,

ρ_ℓ = liquid density, and

g = gravitational acceleration.

The pressure drop refers to the pressure difference between the bottom and the top of the bed.

If surface tension can be ignored (large particles and deep beds), the vapor pressure is equal to the liquid pressure. Equations (2-11) and (2-12) then give

$$\rho_g v_g = (\rho_\ell - \rho_g) g \cdot \frac{\epsilon^3 d^2}{150(1-\epsilon)^2} \cdot \left[\frac{\mu_g}{\rho_g (1-s)^3} + \frac{\mu_\ell}{\rho_\ell s^3} \cdot \frac{\rho_\ell v_\ell}{\rho_g v_g} \right]^{-1} . \qquad (2\text{-}13)$$

For steady countercurrent flow in a bed resting on an impermeable plate,

$$\rho_g v_g = \rho_\ell v_\ell . \qquad (2\text{-}14)$$

so

$$\rho_g v_g = (\rho_\ell - \rho_g) g \cdot \frac{\epsilon^3 d^2}{150(1-\epsilon)^2} \cdot \left[\frac{\mu_g}{\rho_g (1-s)^3} + \frac{\mu_\ell}{\rho_\ell s^3} \right]^{-1} . \qquad (2\text{-}15)$$

The maximum vapor flow is achieved when the derivative of the expression in square brackets in Eq. (2-15) with respect to s is zero, i.e.,

$$\left(\frac{s}{1-s} \right)^4 = \frac{\rho_g \mu_\ell}{\rho_\ell \mu_g} . \qquad (2\text{-}16)$$

The dryout heat flux is given by

$$q_d'' = h_{\ell g} (\rho_g v_g)_{max} \quad , \tag{2-17}$$

where q_d'' is the dryout heat flux and $h_{\ell g}$ is the latent heat of vaporization. After some algebra, the final form of the dryout heat flux expression is

$$q_d'' = (\rho_\ell - \rho_g) g\, h_{\ell g} \cdot \frac{\varepsilon^3}{150(1-\varepsilon)^2} \cdot d^2 \cdot \frac{\rho_g}{\mu_g} \cdot \left[1 + \left(\frac{\rho_g \mu_\ell}{\rho_\ell \mu_g} \right)^{1/4} \right]^{-4} \quad . \tag{2-18}$$

2.1.2 Turbulent Limit

It is well known that, for extremely rough pipes, the pressure drop for turbulent flow through the pipe is proportional to the square of the discharge, independent of the Reynolds number. Particle beds are analogous to interconnected bundles of extremely rough pipes, so one expects that

$$\Delta p/L = \frac{C}{D_H} \cdot \frac{1}{2} \rho v'^2 \tag{2-19}$$

where C is a constant, D_H is the hydraulic diameter of the bed, and v' is the true fluid velocity. Experiments show that for Reynolds numbers [Eq. (2-3)] larger than about 1000, C is indeed a constant and is equal to 7/3.[8] In terms of the diameter, d, of spherical particles, the porosity, ε, and the superficial velocity, v_o, Eq. (2-19) gives

$$\Delta p/L = \frac{1.75(1-\varepsilon)}{d\varepsilon^3} \rho v_o^2 \quad , \tag{2-20}$$

which is the Burke-Plummer equation for the pressure drop in highly turbulent flows through a particle bed.[8] Experimental values of the pressure drop, up to a Reynolds number of 2500, fluctuate by about 15% around the values given by Eq. (2-20).

The change in bed permeability for two-phase turbulent flow through the bed from single phase values is uncertain. Lipinski[5] assumed that it is similar to that for laminar flow, i.e., the vapor pressure drop is enhanced by $1/(1 - s)^3$ and the liquid pressure drop by $1/s^3$, where s is the effective saturation in the bed as defined by Eq. (2-10). Based on the theoretical work of Reed,[9] and also a better fit to recent test data on the dryout heat flux, the exponent 3 was changed to 5. There is also the suggestion that the exponent could be 6.[11,12] To be general, the exponent is denoted by n, so the pressure drop for turbulent flow is

$$\Delta p/L = \rho_g g + \frac{1.75(1 - \epsilon)\,\rho_g v_g^2}{d\epsilon^3 (1 - s)^n}$$

$$= \rho_\ell g - \frac{1.75(1 - \epsilon)\,\rho_\ell v_\ell^2}{d\epsilon^3 s^n} \quad . \tag{2-21}$$

Pressure equality between the phases has been assumed in Eq. (2-21).

At dryout, we again impose the condition that

$$\rho_g v_g = \rho_\ell v_\ell \quad . \tag{2-22}$$

and require that the mass flux $\rho_g v_g$ be maximized with respect to s. The maximum mass flux occurs at

$$\left(\frac{s}{1 - s}\right)^{n+1} = \frac{\rho_g}{\rho_\ell} \quad . \tag{2-23}$$

The dryout heat flux, q_d'', is then reduced to

$$q''_d = h_{\ell g}(\rho_g v_g)_{max}$$

$$= \sqrt{\frac{\rho_g(\rho_\ell - \rho_g) g\, d\, \varepsilon^3}{1.75(1-\varepsilon)}} \cdot h_{\ell g} \cdot \left[1 + \left(\frac{\rho_g}{\rho_\ell}\right)^{\frac{1}{n+1}}\right]^{-\frac{n+1}{2}} . \qquad (2\text{-}24)$$

2.1.3 Laminar-to-Turbulent Transition

The pressure drop data for single phase flow through a particle bed has a scatter of about 20% around the mean value in the laminar-to-turbulent flow transition regime [Reynolds numbers, as defined by Eq. (2-3), between 5 and 1000].[8] The mean value can be represented surprisingly well by the sum of the laminar pressure drop, as given by Eq. (2-7), and the turbulent pressure drop, as given by Eq. (2-20). This is the Ergun equation for pressure drop through a particulate bed.[13]

Combining the laminar and turbulent terms given in Sections 2.1.1 and 2.1.2, respectively (Ergun equation), the pressure drop through the bed is

$$\Delta p/L = \rho_v g + \frac{150\,\mu_g v_g (1-\varepsilon)^2}{\varepsilon^3 d^2 (1-s)^3} + \frac{1.75(1-\varepsilon)\,\rho_g v_g^2}{d\varepsilon^3 (1-s)^n}$$

$$= \rho_\ell g - \frac{150\,\mu_\ell v_\ell (1-\varepsilon)^2}{\varepsilon^3 d^2 (1-s)^3} - \frac{1.75(1-\varepsilon)\,\rho_\ell v_\ell^2}{d\varepsilon^3 (1-s)^n} , \qquad (2\text{-}25)$$

where $3 \leq n \leq 6$.

To simplify the algebra, define

$$q''_{d,L} = h_{\ell g}(\rho_\ell - \rho_g) g \cdot \frac{\varepsilon^3 d^2}{150(1-\varepsilon)^2} \cdot \left[\frac{\mu_g}{\rho_g (1-s)^3} + \frac{\mu_\ell}{\rho_\ell s^3}\right]^{-1} \qquad (2\text{-}26)$$

and

$$q''^{2}_{d,T} = h^{2}_{\ell g}(\rho_\ell - \rho_g)g \cdot \frac{d_c^3}{1.75(1-\epsilon)} \cdot \left[\frac{1}{\rho_g(1-s)^n} + \frac{1}{\rho_\ell s^n}\right]^{-1} , \qquad (2\text{-}27)$$

and applying the condition of steady-state mass balance,

$$\rho_g v_g = \rho_\ell v_\ell , \qquad (2\text{-}28)$$

the equation for the dryout heat flux, q''_d, derived from the above equations is

$$\left(\frac{q''_d}{q''_{d,T}}\right)^2 + \frac{q''_d}{q''_{d,L}} - 1 = 0 , \qquad (2\text{-}29)$$

or

$$q''_d = \left(\frac{q''^{4}_{d,T}}{4\, q''^{2}_{d,L}} + q''^{2}_{d,T}\right)^{1/2} - \frac{q''^{2}_{d,T}}{2\, q''_{d,L}} . \qquad (2\text{-}30)$$

For a given n, q''_d can be obtained numerically by maximizing the expression on the right-hand side of Eq. (2-30) with respect to the effective saturation, s.

For $q''_{d,L} \ll q''_{d,T}$, Eq. (2-30) reduces to

$$q''_d = q''_{d,L} , \qquad (2\text{-}31)$$

and for $q''_{d,T} \ll q''_{d,L}$, Eq. (2-30) reduces to

$$q''_d = q''_{d,T} \quad . \tag{2-32}$$

These are precisely the laminar and turbulent limit dryout heat fluxes given by Eqs. (2-18) and (2-24), respectively, when the appropriate effective saturations are substituted into Eqs. (2-26) and (2-27) to maximize the heat fluxes.

In the laminar regime, the expression for the turbulent limit dryout heat flux overestimates the dryout heat flux [see the condition leading to Eq. (2-31)], and in the turbulent limit, the expression for the laminar dryout heat flux also overestimates the dryout heat flux [see the condition leading to Eq. (2-32)]. So in the transition from laminar to turbulent flow, the dryout heat flux is less than that predicted by either the laminar or the turbulent flow models.

2.2 Dryout Heat Flux Based on Flooding

The flooding experiments reported in the literature were performed mostly with Raschig rings (thick-walled hollow cylinders whose heights are approximately equal to their diameters) and Berl saddles (saddle-shaped particles) dumped in towers over a meter in height. Sherwood, et al.[14] first introduced two dimensionless parameters to correlate the flooding data. These are

$$x = \frac{v_\ell}{v_g}\sqrt{\frac{\rho_\ell}{\rho_g}} = \frac{\rho_\ell v_\ell}{\rho_g v_g}\sqrt{\frac{\rho_g}{\rho_\ell}} \quad , \tag{2-33}$$

and

$$y' = \frac{v_g^2 S}{g\varepsilon^3} \cdot \frac{\rho_g}{\rho_\ell} \quad , \tag{2-34}$$

where the velocities are superficial velocities and S is the surface area of the packed particles per unit bed volume. Two powers in the exponent of ε^3 in Eq. (2-34) come from expressing the true fluid velocity, v', in

terms of the superficial velocity, v_g, and one power from the ratio of the fluid volume to the bed volume. [The factor y' is in fact proportional to v'^2/gD_H, where D_H is the hydraulic diameter defined by Eq. (2-2).]

To correlate data obtained with various liquids, it was found necessary to modify y' to y, defined by

$$y = y' \mu^{0.2}$$

$$= \frac{v_g^2 S}{g_c^3} \cdot \frac{\rho_g}{\rho_\ell} \cdot \mu_\ell^{0.2} \quad . \tag{2-35}$$

where μ_ℓ is the dynamic viscosity of the liquid. (Note that after the above change, y is no longer a dimensionless parameter.) A plot of Sherwood's correlation (y vs. x), with μ_ℓ expressed in units of 10^{-3} Pa-s (centipoise), is shown in Fig. 2.

2.2.1 Dryout Heat Flux from Direct Flooding Correlation

The parameter y, given by Eq. (2-35), contains a factor proportional to the square of the vapor flux through the particle bed $\left(v_g^2\right)$. If the dryout heat flux is directly proportional to the vapor flux determined by the flooding line, the Sherwood correlation can be used to obtain the dryout heat flux.

For a particle bed resting on an impermeable plate, the mass conservation for a steady-state flow pattern requires

$$\rho_g v_g = \rho_\ell v_\ell \quad . \tag{2-36}$$

The parameter x, as defined by Eq. (2-33) then becomes

$$x = \sqrt{\frac{\rho_g}{\rho_\ell}} \quad . \tag{2-37}$$

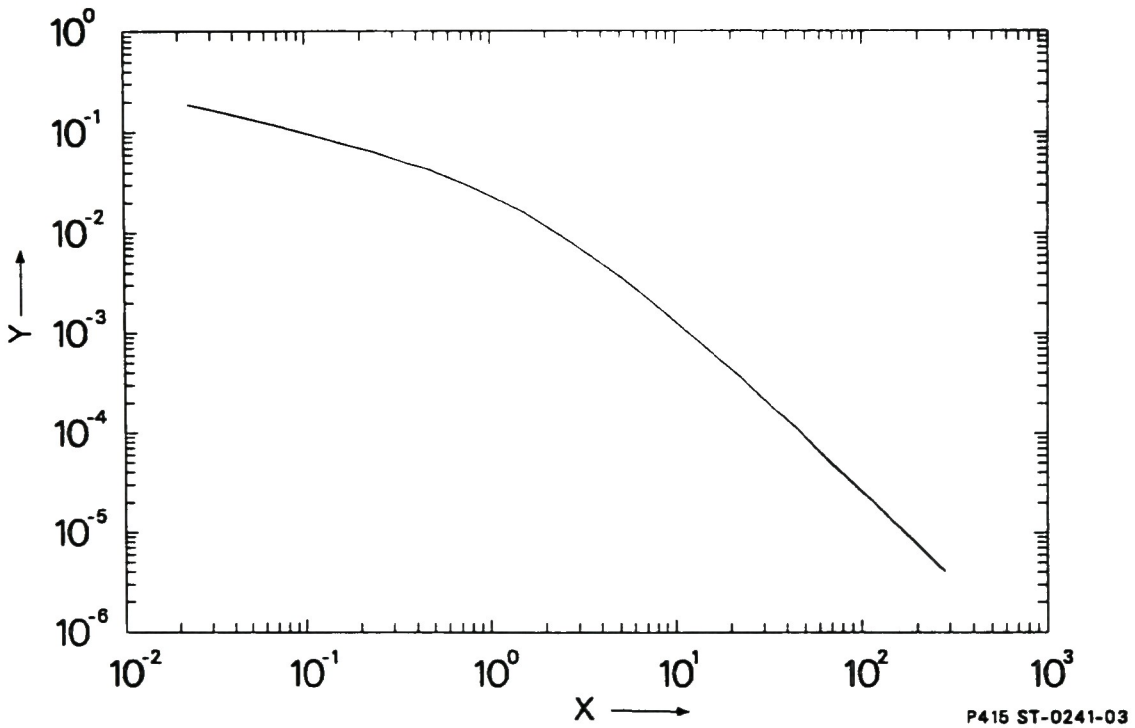

Figure 2. Flooding correlation (from Sherwood, et al.[14]); see Eqs. (2-37) and (2-35) for definitions of X and Y, respectively.

Since $\rho_g << \rho_\ell$, one needs be concerned with only the left end of the correlation curve shown in Figure 2. In this region

$$y \sim x^{-1/2} \quad . \tag{2-38}$$

The constant of proportionality can be obtained by extrapolating the curve to $x = 0.01$ and $y = 0.3$. So

$$y = 0.03x^{-1/2} \quad . \tag{2-39}$$

In terms of physical parameters, Eq. (2-39) becomes

$$\rho_g^2 v_g^2 \cdot \frac{S}{g_c^3} \cdot \frac{1}{\rho_\ell \rho_g} \cdot \mu_\ell^{0.2} = 0.03\left(\frac{\rho_\ell}{\rho_g}\right)^{1/4} \quad . \tag{2-40}$$

The dryout heat flux, q_d'', is

$$q_d'' = h_{\ell g} \rho_g v_g$$

$$= \sqrt{0.03}\, h_{\ell g} \sqrt{\frac{\rho_g \rho_\ell g_c^3}{S}} \left(\frac{\rho_\ell}{\rho_g}\right)^{1/8} \mu_\ell^{-0.1} \quad . \tag{2-41}$$

The surface area per unit bed volume, S, is related to the porosity and the specific area of the particles (particle surface area divided by particle volume), S_p, as

$$S = (1 - \epsilon)S_p \quad . \tag{2-42}$$

For spherical particles of diameter d,

$$S_p = \frac{6}{d} \quad . \tag{2-43}$$

For nonspherical particles, we can define an equivalent diameter as

$$d = f \cdot \frac{6}{S_p} \quad , \tag{2-44}$$

where f is a shape factor less than 1.

Substituting for S in terms of the particle diameter into Eq. (2-41), gives

$$q_d'' = \sqrt{0.005}\, h_{\ell g} \sqrt{\frac{\rho_g \rho_\ell g d \varepsilon^3}{(1-\varepsilon) f}} \left(\frac{\rho_\ell}{\rho_g}\right)^{1/8} \mu_\ell^{-0.1} \quad . \tag{2-45}$$

Putting f = 1 and expressing μ_ℓ in units of the dynamic viscosity of saturated water at one atmosphere, μ_w (2.82×10^{-4} Pa-s), we obtain the Sowa equation:[7]

$$q_d'' = 0.080\, h_{\ell g} \sqrt{\frac{\rho_g \rho_\ell g d \varepsilon^3}{1-\varepsilon}} \left(\frac{\rho_\ell}{\rho_g}\right)^{1/8} \left(\frac{\mu_w}{\mu_\ell}\right)^{0.1} \quad . \tag{2-46}$$

Putting f = 1 and expressing μ_ℓ in units of the dynamic viscosity of water at room temperature and pressure, μ_o (1.00×10^{-3} Pa-s), we obtain the Theofanous equation:[15]

$$q_d'' = 0.071\, h_{\ell g} \cdot \sqrt{\frac{\rho_g \rho_\ell g d \varepsilon^3}{1-\varepsilon}} \left(\frac{\rho_\ell}{\rho_g}\right)^{1/8} \left(\frac{\mu_o}{\mu_\ell}\right)^{0.1} \quad . \tag{2-47}$$

The above two equations are in fact equivalent. Because both neglect the shape factor for nonspherical particles upon which the correlation was based, they tend to underpredict the dryout heat flux when applied to spherical particles.

2.2.2 Dryout Heat Flux from Transformed Flooding Correlation

The Sherwood Correlation (Fig. 2) can be better represented algebraically over its entire range if the following transformation is carried out. That is, let

$$\xi = y^{1/2} \quad \text{and} \quad \eta = xy^{1/2} \quad . \tag{2-48}$$

When $\eta^{1/2}$ is plotted against $\xi^{1/2}$, a linear relationship is obtained. A good fit to the data[16] is

$$\xi^{1/2} + \eta^{1/2} = 0.775 \quad , \tag{2-49}$$

The dynamic viscosity has been expressed in units of 10^{-3} Pa-s (centipoise). The above form is remarkably similar to the theoretical limit of stable, stratified channel flow.[17] Expressing ξ and η in terms of physical parameters and the dynamic viscosity in SI units, Eq. (2-49) gives

$$\left[\rho_g^{\,2} v_g^{\,2} \cdot \frac{S}{g c^3} \cdot \frac{1}{\rho_g \rho_\ell}\right]^{1/4} + \left[\rho_\ell^{\,2} v_\ell^{\,2} \cdot \frac{S}{g c^3} \cdot \frac{1}{\rho_\ell^{\,2}}\right]^{1/4} = 0.775 \left(\frac{10^{-3}}{\mu_\ell}\right)^{0.05} \quad . \tag{2-50}$$

Again applying the condition $\rho_g v_g = \rho_\ell v_\ell$ and $q_d'' = \rho_g v_g h_{\ell g}$, we obtain

$$q_d'' = (0.775)^2 \cdot h_{\ell g} \cdot \sqrt{\frac{\rho_g \rho_\ell g c^3}{S}} \cdot \left[1 + \left(\frac{\rho_g}{\rho_\ell}\right)^{1/4}\right]^{-2} \cdot \left(\frac{10^{-3}}{\mu_\ell}\right)^{0.1} \quad . \tag{2-51}$$

Using Eqs. (2-42) through (2-44), assuming unity for the shape factor, f, and 10^{-3} Pa-s for the liquid dynamic viscosity, the Ostensen-Lipinski equation[18] is obtained:

$$q_d'' = 0.245\, h_{\ell g} \sqrt{\frac{\rho_g \rho_\ell g d \varepsilon^3}{1-\varepsilon}} \cdot \left[1 + \left(\frac{\rho_g}{\rho_\ell}\right)^{1/4}\right]^{-2} . \qquad (2\text{-}52)$$

Like the Sowa or the Theofanous model, because of its neglect of the shape factor for nonspherical particles upon which the correlation was based, the Ostensen-Lipinski model underpredicts the dryout heat flux when applied to spherical particles. Moreover, because the dynamic viscosity of saturated water decreases by an order of magnitude at high temperatures, neglect of the viscosity term may substantially underpredict the dryout heat flux for a particle bed immersed in water.

It is interesting to note that the Lipinski turbulent-limit model with n = 3 [Eq. (2-24)] gives

$$q_d'' = 0.756\, h_{\ell g} \sqrt{\frac{\rho_g (\rho_\ell - \rho_g)\, g d \varepsilon^3}{1-\varepsilon}} \left[1 + \left(\frac{\rho_g}{\rho_\ell}\right)^{1/4}\right]^{-2} , \qquad (2\text{-}53)$$

essentially differing in only a coefficient (though quite substantial) from Eq. (2-52).

2.2.3 An Extended Model Based on Flooding

The presence of the viscosity term in the Sherwood correlation [Eq. (2-40) or (2-49)] suggests that the flooding data were obtained in a flow regime where the liquid flow in the bed was not completely turbulent. To make the correlation completely dimensionless, one can replace the term involving the liquid viscosity, μ_ℓ, by the liquid Reynolds number, Re_ℓ, which is given by

$$Re_\ell = \frac{3}{2}\, \rho_\ell v_\ell' D_H / \mu_\ell , \qquad (2\text{-}54)$$

analogous to Eq. (2-3).

The true liquid velocity, v_ℓ', is expected to be on the order of the velocity attained in a free fall over a distance of a hydraulic diameter, D_H. Therefore,

$$Re_\ell \sim \rho_\ell \sqrt{g\, D_H}\, D_H / \mu_\ell \sim \rho_\ell \sqrt{g(\epsilon/S)^3} / \mu_\ell \quad . \tag{2-55}$$

where the hydraulic diameter is replaced by ϵ/S; ϵ is the porosity, and S is the particle surface area per unit bed volume, as defined earlier.

The correlation we seek involves the parameters

$$x = \frac{\rho_\ell v_\ell}{\rho_g v_g} \sqrt{\frac{\rho_g}{\rho_\ell}} \quad \text{and} \quad y_1 = \frac{v_g^2 S}{g\epsilon^3} \cdot \frac{\rho_g}{\rho_\ell} \cdot \left(\frac{\mu_\ell}{\lambda_\ell}\right)^{0.2} \quad , \tag{2-56}$$

where λ_ℓ is defined as

$$\lambda_\ell = \rho_\ell \sqrt{g\epsilon^3/S^3} \quad . \tag{2-57}$$

In the Wallis form, these parameters are transformed to

$$n_1^2 = x^2 y_1$$

$$= \rho_\ell^2 v_\ell^2 \cdot \frac{S}{g\epsilon^3} \cdot \frac{1}{\rho_\ell^2} \cdot \left(\frac{\mu_\ell}{\lambda_\ell}\right)^{0.2} \quad \text{and}$$

$$\xi_1^2 = y_1$$

$$= \rho_g^2 v_g^2 \cdot \frac{S}{g\epsilon^3} \cdot \frac{1}{\rho_g \rho_\ell} \cdot \left(\frac{\mu_\ell}{\lambda_\ell}\right)^{0.2} \tag{2-58}$$

Based on the data of Sherwood, et al.,[14] Uchida and Fujita,[19] and those published by White,[6] together with the values of S/ε^3 given by Lobo, et al.[20] for these experiments, a linear regression between $\eta_1^{1/2}$ and $\xi_1^{1/2}$ gives

$$\xi_1^{1/2} + 0.939\ \eta_1^{1/2} = 0.549 \quad . \tag{2-59}$$

The root-mean-square (RMS) deviation of the data points from the regression line is 0.03. Most of the scatter comes from the data given by White.[6] The data and the regression line are plotted in Fig. 3.

To obtain the dryout heat flux of a particle bed resting on an impermeable plate, we again apply the conditions

$$\rho_g v_g = \rho_\ell v_\ell \tag{2-60}$$

and

$$q_d'' = \rho_g v_g h_{\ell g} \quad . \tag{2-61}$$

Equation (2-59) then gives

$$q_d'' = (0.549)^2\ h_{\ell g} \sqrt{\frac{\rho_g \rho_\ell g \varepsilon^3}{S}} \cdot \left[\frac{\rho_\ell}{\mu_\ell} \cdot \sqrt{\frac{g\varepsilon^3}{S^3}}\right]^{0.1} \cdot \left[1 + 0.939 \left(\frac{\rho_g}{\rho_\ell}\right)^{1/4}\right]^{-2} \quad . \tag{2-62}$$

Introducing a shape factor, f, for Raschig rings (all data used are those obtained with Raschig rings), and converting S to an equivalent diameter of spherical particles, we have

$$S = (1 - \varepsilon)\ S_p$$

$$= (1 - \varepsilon) \cdot \frac{6f}{d} \quad . \tag{2-63}$$

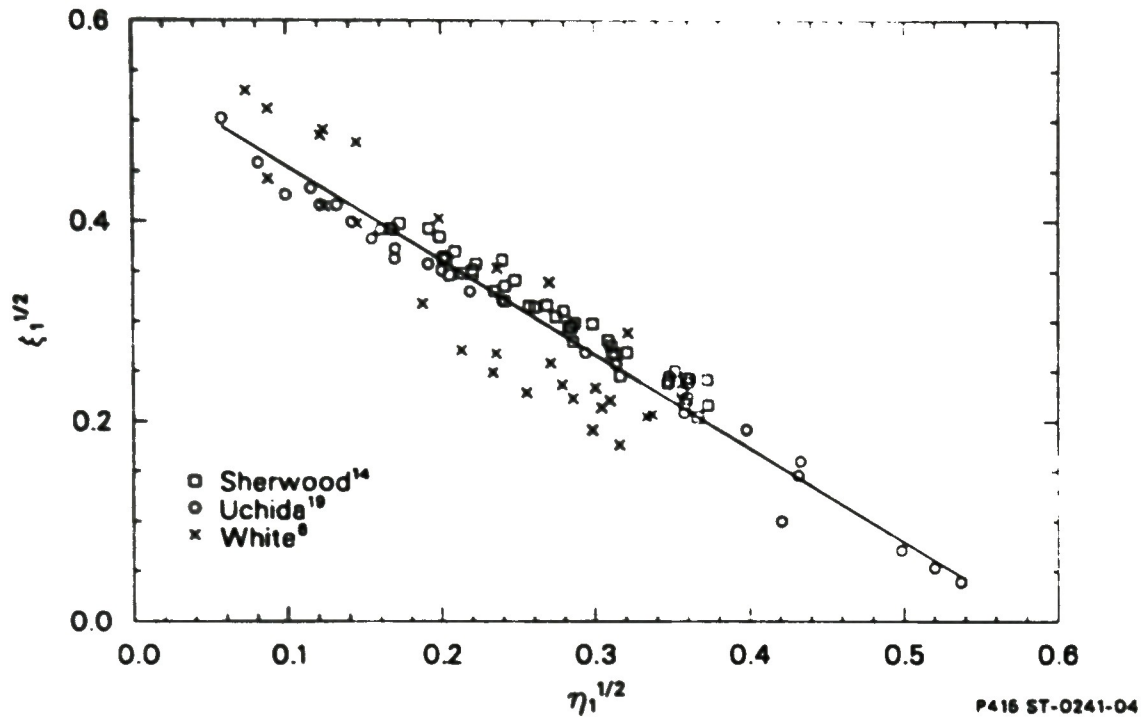

Figure 3. Flooding correlation based on two dimensionless parameters, η_1 and ξ_1; see Eq. (2-58) for definitions of η_1 and ξ_1.

The correlation for q_d'' becomes

$$q_d'' = 0.094\, h_{\ell g} \sqrt{\frac{\rho_g \rho_\ell g d \epsilon^3}{(1-\epsilon)f}} \cdot \left(\frac{\rho_\ell}{\mu_\ell} \cdot \frac{d}{(1-\epsilon)f} \cdot \sqrt{\frac{g d \epsilon^3}{(1-\epsilon)f}} \right)^{0.1}$$

$$\cdot \left[1 + 0.939 \left(\frac{\rho_g}{\rho_\ell} \right)^{1/4} \right]^{-2} . \qquad (2\text{-}64)$$

Based on the RMS deviation of the data points from the regression line, the error expected for q_d'', given by Eq. (2-64), is about 12%.

In developing the correlation, we have neglected the buoyancy force on the liquid due to the presence of the gas. To take this into account, the gravity g should be replaced by $\left(1 - \rho_g/\rho_\ell\right)g$. Because the gas density is much lower than the liquid density in the experimental data base, such a refinement will not affect the correlation coefficients. At high pressures, as the steam density is increased substantially relative to the liquid density, the neglect of the buoyancy force may introduce an error on the order of a few percent.

Based on the definition of the Reynolds number given by Eq. (2-3), the experimental data base spans a range of liquid Reynolds numbers from 2.5 (Sherwood data) to 1600 (White data).

2.3 Comparison with Experiments

A full assessment of the models presented above involves experiments which systematically vary the porosity of the particle bed, the diameter of the particles composing the bed, and the ratio of the vapor-to-liquid density (system pressure). Before the TMI-2 accident, most of the experimental emphasis was on shallow beds composed of fine particles which were believed to be applicable to rubble beds formed during an hypothetical core disruptive accident in a liquid-metal fast-breeder reactor. For these beds, the flow conditions at dryout are in the laminar regime, and the

dryout is strongly influenced by capillary forces and the formation of vapor channels near the top of the beds.[5] Obviously, these experiments are not suitable for making comparisons with the model predictions for deep beds composed of large particles. Data on deep beds are scarce and cover only a small range of porosity around 0.4. Therefore, the following comparison is quite limited in extent, although it appears surprisingly good.

The Sandia Laboratory's Degraded Core Coolability experiment DCC-2 is an in-pile experiment performed in the Annular Core Research Reactor.[21] The bed had a height of 0.49 m, which can be considered as a deep bed, and consisted of particles averaging 1.42 mm in diameter based on the Fair-Hatch formula (harmonic mean weighted by mass fraction). The porosity was reported to be 0.41. Volumetric heating was achieved by fission driven by neutrons supplied from the reactor. The data cover a range of pressures from 0.26 MPa to 16 MPa.

Figure 4 shows a comparison between the DCC-2 data and the model predictions. During the DCC-2 experiment, two distinct dryouts were noted at any particular pressure; one was a local dryout and the other, somewhat higher in the dryout heat flux, was a global dryout. The local dryout was believed to be caused by a local concentration of smaller particles, which decreased the local permeability relative to the rest of the bed. The data points given in Fig. 3 are the local dryout heat fluxes. The global dryout heat fluxes follow a similar trend.

The Lipinski model predictions in Fig. 4 were computed from Eq. (2-30), the dryout heat flux in the laminar-to-turbulent flow regime, with the appropriate substitutions for $q''_{d,L}$ and $q''_{d,T}$ given by Eqs. (2-26) and (2-27), respectively. Two turbulent permeability models were used, one with $n = 5$ and the other with $n = 6$, as shown in Eq. (2-27). At low pressures (small liquid Reynolds number), the difference between the two models is small, but the $n = 5$ model gives a maximum dryout heat flux that is 30% higher than that given by the $n = 6$ model at pressures around 5 MPa.

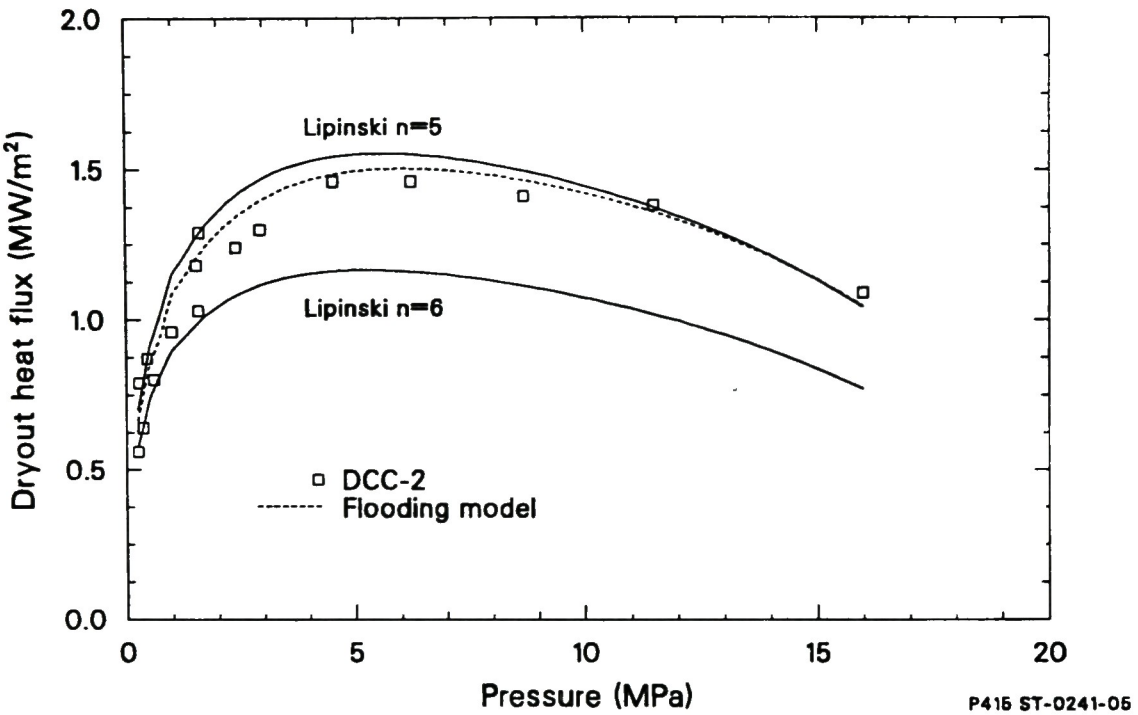

Figure 4. Dryout heat flux model comparison to DCC-2 experiment.

The flooding model, based on flooding experiments [Eq. (2-64)], has an undetermined shape factor for Raschig rings. If f is taken to be 0.42, the correlation gives excellent agreement with the DCC-2 local dryout data over the entire range of pressures. The formula plotted to give the curve labeled "flooding model" in Fig. 4 is obtained from Eq. (2-64) with the substitution of 0.42 for f and $\left(1 - \rho_g/\rho_\ell\right)g$ for g, i.e.,

$$q_d'' = 0.165\, h_{\ell g} \sqrt{\frac{\rho_g \left(\rho_\ell - \rho_g\right) g d_c^3}{1 - \varepsilon}} \cdot \left[\frac{\rho_\ell d}{(1 - \varepsilon)\,\mu_\ell} \cdot \sqrt{\frac{\left(1 - \rho_g/\rho_\ell\right) g d_c^3}{1 - \varepsilon}}\right]^{0.1}$$

$$\cdot \left[1 + 0.939 \left(\frac{\rho_g}{\rho_\ell}\right)^{1/4}\right]^{-2} \quad . \tag{2-65}$$

The liquid Reynolds number at dryout computed from the flooding model varies from 2.6 to 26. This is within the range of the data base for the flooding correlation.

Figure 5 compares the model predictions given by the flooding model [Eq. (2-65)] with other dryout data for deep beds for liquid Reynolds numbers between 2.8 and 70. Both the Winfrith[22] and the Westinghouse[23] data do not have reported porosities which, nevertheless, are believed to be around 0.4, typical of such experiments. In the model predictions, the porosities are assumed to follow the relationship given by Barleon and Werle,[24] i.e.,

$$\varepsilon = 0.373 + 0.0063\, d \quad , \tag{2-66}$$

where d is in mm. Porosities for the KfK[25] data are those as given in the reference. Cylindrical particles are converted to equivalent spherical particles with a shape factor equal to 0.78. The RMS difference between experimental data and the model predictions is only 12%. Considering the diverse source of the data base, this is quite a remarkable agreement.

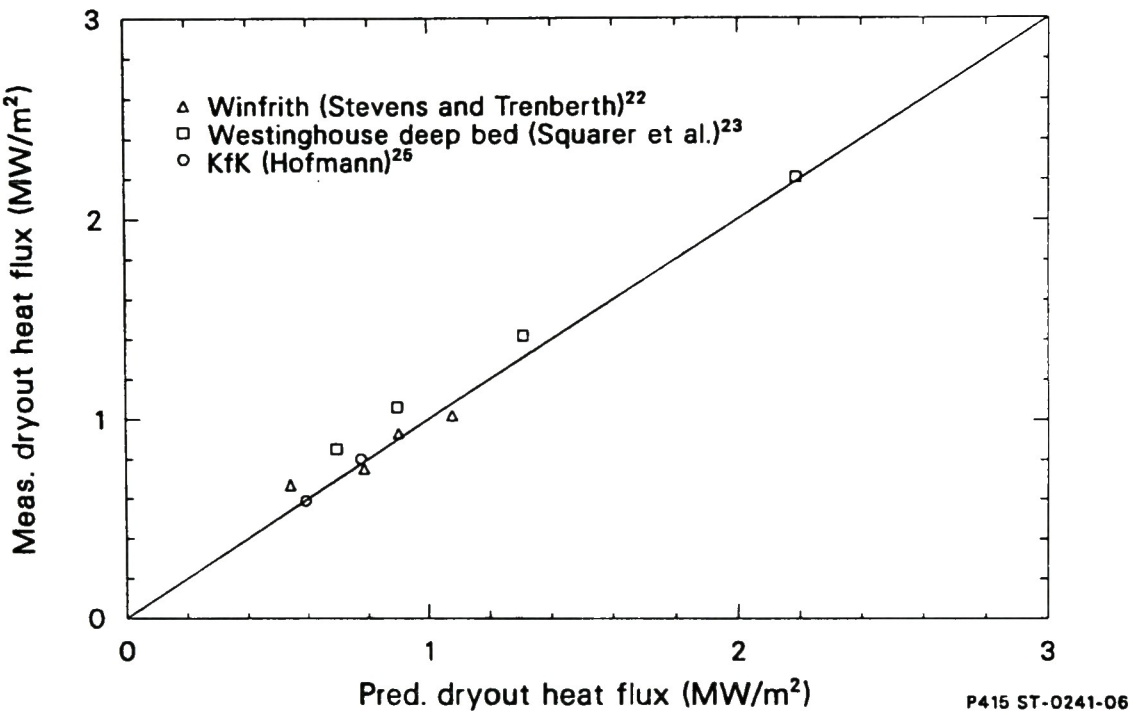

Figure 5. Comparison between predicted (extended flooding model) and experimental dryout heat fluxes for deep particle beds.

Most of the data points in Fig. 5 were obtained by digitizing the plots given in the references. For easier reference, the data points and other relevant information are given in Table 1.

Although the agreement between the model predictions and the experimental data presented here is very good, a word of caution is in order. The model only applies to deep beds and considerably underpredicts the dryout heat fluxes for shallow beds. For example, the Barleon, Thomauske, and Werle[26] data for beds composed of large particles (2 to 16 mm) give about 40% higher dryout heat fluxes than predicted by Eq. (2-65), apparently due to the shallowness of the beds (less than 0.1 m deep). Also, the correlation based on the flooding data applies only to a range of liquid Reynolds numbers (at dryout) between 2.5 and 1600.

2.4 Dryout of the TMI-2 Upper-Core Particle Bed

As mentioned in the Introduction section, the damaged TMI-2 core gave rise to two distinct particle beds, one in the core region above a consolidated crust and one in the lower plenum, resting on the lower head. Since defueling of the reactor, much has been learned about the upper-core particle bed but, except for some visual observations, little is known about the lower plenum particle bed. The top layer of the lower plenum particle bed appears loose but is quite heterogeneous. There are regions consisting of very fine particles, which are easily moved by a jet of water, as well as regions covered with solidified, previously molten debris of core material up to 0.2 m in extent. It is unclear whether the particle bed extends to the vessel head or there exists a layer of solid material between the top layer of the particle bed and the vessel head. Because of this lack of proper characterization of the lower plenum particle bed, this report only addresses the upper-core particle bed.

The upper-core particle bed covered most of the core. A good approximation to a horizontal cross-section through the middle of the bed is that of a circular plate with a diameter equal to 13 fuel assemblies (2.84 m). The bottom of the particle bed has been determined by driving a

TABLE 1. DRYOUT HEAT FLUX FOR DEEP PARTICLE BEDS AT 1 ATMOSPHERE

Diameter (mm)	Porosity	D.O. Heat Flux (measured) (MW/m^2)	Source	D.O. Heat Flux (predicted)[a] (MW/m^2)	Liquid Reynolds Number
2.0	0.386[b]	0.67	Winfrith[22]	0.54	2.8
3.4	0.394[b]	0.75	"	0.79	7.0
4.0	0.398[b]	0.93	"	0.90	9.4
5.0	0.405[b]	1.02	"	1.08	14.2
2.84	0.391[b]	0.85	Westinghouse[23]	0.69	5.1
3.97	0.398[b]	1.06	"	0.90	9.3
6.35	0.413[b]	1.42	"	1.31	22.3
11.1	0.443[b]	2.21	"	2.19	68.6
2.34	0.385	0.59	KfK[25]	0.59	3.5
3.00	0.405	0.80	"	0.77	6.1

a. Computed from Eq. (2-65).

b. Computed from Eq. (2-67).

pointed tool into the bed until it hits the top crust of the consolidated region.[27] The top surface has been determined by two methods, one employing an acoustic reflection technique before the removal of the reactor upper head,[28] and the other by lowering a pointed tool through the reactor cavity until it touches the bed.[27] With the acoustic method, the average height of the particle bed is determined to be 1.05 m and the volume is equal to 6.68 m^3.[29] With the probing method, the average height is 0.80 m,[2] and the volume is 5.06 m^3.

Based on the TMI-2 reactor defueling log, the amount of material removed from the particle bed is 23,700 kg.[30] Thus, the average density of the particle bed is 3550 and 4680 kg/m^3, respectively, based on the two volume determinations as mentioned above. [These fall within the range of density determinations of samples of the particles in the laboratory (3500 to 5500 kg/m^3).[31]] Examination of the particles showed that they are mostly fractured fuel pellets and oxidized cladding.[31] Based on the composition (U/Zr = 7 by mass), the density of an average particle is expected to be about 9000 kg/m^3. If the average of the two bed densities is used, the porosity of the bed is deduced to be 0.54.

Eleven samples of particles were taken from various depths of the upper-core particle bed in 1983 and 1984. Particle size distribution was obtained for nine of these samples. Table 5 of Ref. 31 gives the detailed distribution of the weight fraction as a function of the particle size. This is adapted in Table 2 with the minor modification of substituting the mid-point of a range of particles sizes for the actual reported range. In the context of particle bed dryout, the proper average for particle size is the harmonic mean weighted by the volume fraction, or the weight fraction when the particles have a uniform density. With such an average, a particle bed consisting of same-sized particles as the average particle gives the same surface area per unit volume as the bed of a mixture of particles of different sizes from which the average is obtained. Because the TMI-2 particles are not spherical, to convert them to effective spherical particles of diameter d, we apply a shape factor of 0.78 to the average (Fair-Hatch formula, see Ref. 5). Therefore, we have

TABLE 2. WEIGHT DISTRIBUTION OF SAMPLES OF THE TMI-2 CORE PARTICLE BED
(weight in g)

Sieve Size (mm)	Sample 1	Sample 3	Sample 5	Sample 6	Sample 7	Sample 8	Sample 9	Sample 10	Sample 11
4.500	12.62	63.75	69.57	57.99	7.38	28.39	5.69	15.93	30.58
2.840	27.82	51.45	13.96	49.39	59.44	74.55	53.81	88.03	57.44
1.640	15.64	19.19	6.25	13.88	43.29	28.91	30.63	33.56	21.20
0.854	7.80	5.49	0.44	8.93	13.48	9.13	16.18	11.59	10.89
0.502	3.20	6.34		5.99	9.77	7.49	25.31	14.76	16.90
0.223	0.87	1.27		0.97	0.89	1.35	9.03	3.96	6.57
0.112	0.44	0.77		0.67	0.54	0.95	5.34	1.78	2.91
0.052	0.17	0.19		0.22	0.37	1.80	6.62	1.36	2.03
Total Weight	68.56	148.45	90.22	138.04	135.16	152.57	152.61	170.97	148.52
Effective Diameter (mm)	1.05	1.41	2.75	1.39	0.99	0.92	0.36	0.82	0.63

$$d = 0.78W\left(\sum_i W_i/d_i\right)^{-1} \quad . \tag{2-67}$$

where W is the weight of each sample, and W_i is the weight of particles in the sample having sieve diameter d_i. The effective diameters of the samples are listed in Table 2. When all the samples are normalized to the same weight, the effective diameter of the particles in all the samples is found to be 0.87 mm.

Based upon the above discussion, the characteristics of the particle bed in the TMI-2 core, reduced to the form of a right-circular cylinder, are summarized in Table 3.

The particle bed in the TMI-2 core is large and deep enough that models of the dryout heat flux given in previous sections are expected to be applicable, at least in the central regions of the bed far away from its periphery. Because the flooding model [Eq. (2-65)] compares well with experiments on deep beds and also with the Lipinski n = 5 model in the laminar-to-turbulent transition regime [Eq. (2-30)], we have computed the dryout heat flux of the bed as a function of pressure from these two models. The primary system pressure history during the accident is shown in Fig. 6 for the period between 175 min, when the particle bed presumably was formed by the action of the 2-B primary coolant pump, and 300 min, shortly before system pressurization. The times are measured from the time of turbine trip. With this pressure history, the computed dryout heat fluxes are shown in Fig. 7 as functions of time. The liquid Reynolds number [Eq. (2-3)] varies between 30 and 40 for the dryout heat fluxes shown, well inside the range of the flooding correlation upon which the flooding model is based. As shown in Fig. 7, the results of the Lipinski n = 5 model and the flooding model differ by at most 3% over the entire period.

To determine the coolability of the particle bed, the dryout heat flux was compared to the heat flux from decay heat generated within the particle

TABLE 3. CHARACTERISTICS OF THE TMI-2 UPPER-CORE PARTICLE BED (reduced to the form of a right-circular cylinder)

Height	0.93 m
Diameter	2.84 m
Cross-section area	6.33 m^2
Volume	5.89 m^3
Particle diameter	0.87 mm
Porosity	0.54
Particle surface area per unit volume	3170 m^{-1}
Total particle surface area	18,700 m^2
Total mass	23,700 kg
UO_2 mass	20,300 kg

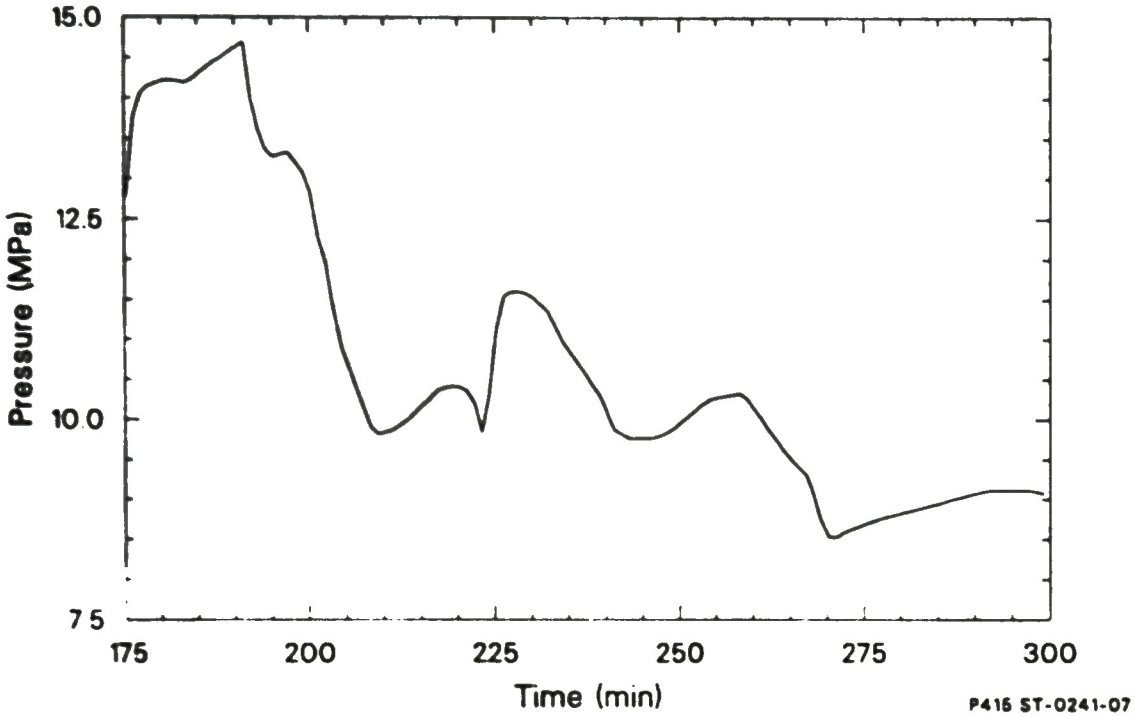

Figure 6. Primary system pressure history; time is measured from the time of turbine trip.

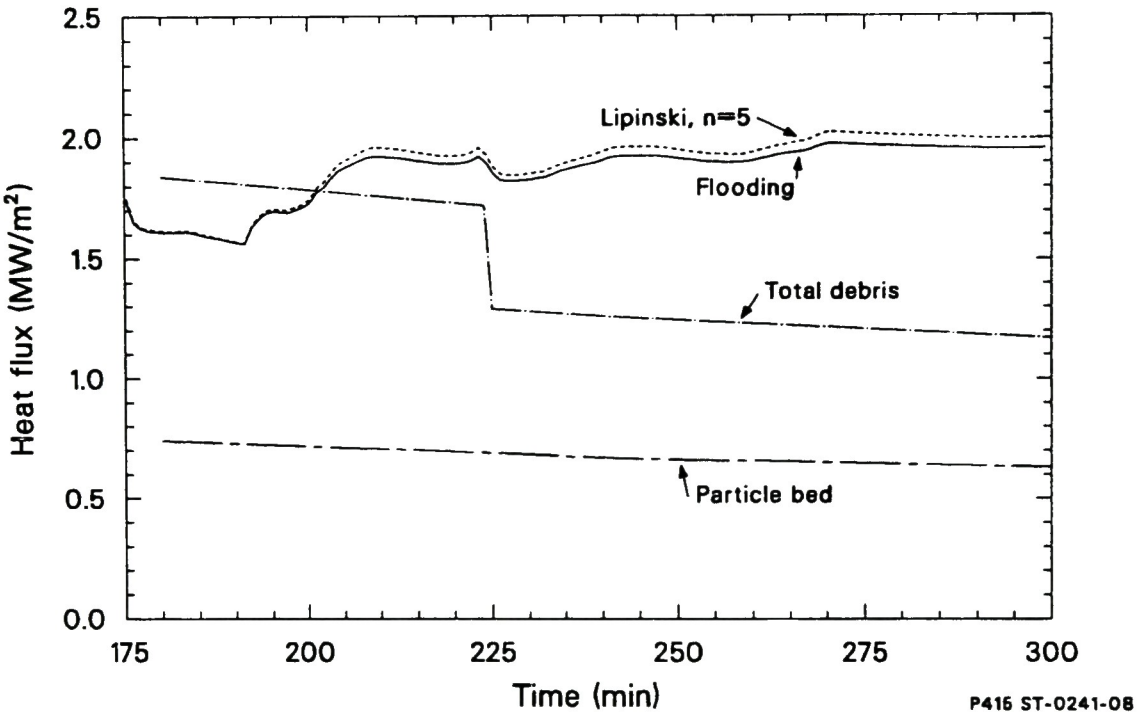

Figure 7. Comparison of predicted dryout heat fluxes with heat fluxes from decay heat generation.

bed plus that transferred to it from the consolidated region below. The fuel content in the particle bed has already been estimated and is given in Table 3. The fuel content in the consolidated region before the relocation to the lower plenum at 225 min can be estimated as follows. From post-accident examination of the core, the amount of material still in the form of rods is estimated to be 54,600 kg.[29] The total core material before the accident was 123,000 kg.[32] Therefore, the damaged core material in the form of debris is 68,400 kg. Based on a fuel loading of 93,100 kg, the fuel content in the debris is 51,800 kg. Subtracting the fuel content of 20,300 kg in the particle bed (Table 3), the fuel content in the consolidated debris before relocation was 31,500 kg. The material content in the consolidated region after relocation (end-state configuration) has not been determined. However, based on volume and density estimates, its mass is about 24,000 kg.[29] Assuming the fuel fraction is the same as the intact core, the mass of fuel in the consolidated debris after relocation is about 18,200 kg. The fuel mass distribution in the core debris is summarized in Table 4, which also shows the fractional core power in the debris. It has been assumed that the power per unit fuel mass in the particle bed is the same as the core average and, in the consolidated region, it is 20% higher.

To determine the coolability of the core particle bed, the dryout heat flux was compared to the heat generation in the particle bed as well as heat transferred to it from the consolidated region. Assuming a 50% release of the more volatile fission products from the core debris, the decay heat generation rates in the consolidated region and in the particle bed are given in Table 5 for the time period between 180 and 300 min.[2] The decrease in power in the consolidated region at 225 min is based on a reduction of 13,300 kg of fuel. If all the heat generated in the particle bed is transferred upwards, it would give a heat flux of approximately 0.7 MW/m^2 at the top surface of the bed during the 180 to 300 min period. This is shown in Fig. 7 along with the predicted dryout heat fluxes. Also shown in Fig. 7 is the heat flux at the top of the particle bed if 80% of the heat generated in the consolidated region is also transferred upwards through the particle bed. Before 225 min, this latter heat flux was comparable to the predicted dryout heat fluxes, so the

TABLE 4. CORE DEBRIS MASS AND POWER DISTRIBUTION

	Before 225 min		After 225 min	
	UO_2 Mass (kg)	Fractional Core Power	UO_2 Mass (kg)	Fractional Core Power
Particle Bed	20,300	0.218	20,300	0.218
Consolidated Region	31,500	0.406	18,200	0.235

TABLE 5. POWER HISTORY IN CORE DEBRIS

Time (min)	Power in Consolidated Region (MW)	Power in Particle Bed (MW)
180	8.69	4.67
225^-	8.16	4.38
225^+	4.72	4.38
240	4.61	4.27
300	4.28	3.97

particle bed may be on the verge of dryout if covered with water. After 225 min, with a reduction in power from the consolidated region, this heat flux would have dropped to approximately 0.5 MW/m^2 below the predicted dryout heat fluxes, indicating that the bed would not have dried out if covered with water.

The upper-core particle bed, however, is believed to have been formed at high temperature and to have remained dry until it was finally quenched with emergency core cooling water. In addition to the analysis of its dryout heat flux, which shows that the particle bed would not have dried out after being covered with water, a quenching analysis is needed to complete the description of its thermal behavior. This is described in the next section.

3. PARTICLE BED QUENCHING

3.1 Review of Quenching Experiments

The quenching of particle beds from a high temperature state has not been studied in as much detail as the dryout of particle beds. The early experiments of Ginsberg, et al.,[33,34,35] and of Cho, Armstrong, and Chan[36] showed that with large particles (~3 mm), the average heat flux at the top of the particle bed during quench is comparable to the dryout heat flux of the bed and is independent of the temperature from which the bed is quenched. The pattern of the quench front, however, is quite complicated. In a top-down quench, a liquid column first penetrates the center of the bed, leaving the outside annulus of the bed dry until the liquid reaches the bottom of the bed. Then a second quench front propagates upward in the annulus as the bed is being filled with water from the central region. In general, the downward-propagating quench front moves faster than the upward-propagating front, but the cross-section area of the former is smaller than that of the latter. This results in approximately the same heat flux during both the downward and the upward quench.

The quench behavior observed in experiments with large particles, however, is not confirmed in the quenching of particle beds with smaller particles.[37] With smaller particles, the top-down quench front is one-dimensional and progresses uniformly downward over the entire cross-section of the bed. Moreover, the heat flux from the particle bed during quenching is considerably less than the measured dryout heat flux for the bed. In the Sandia Degraded Core Coolability experiments,[21,38] mixtures of particles of various sizes were used. Again, with smaller particles (DCC-1), the quench front was observed to be uniform across the bed and the heat flux at the quench front was estimated to be a few times lower than the measured dryout heat flux. With larger particles (DCC-2 and DCC-3), the quenching was nonuniform, but the quench heat flux was still a few times lower than the dryout heat flux, in contrast with the results for particle beds having uniform-sized particles.

No adequate theory has been proposed to explain the difference in the quenching behavior of particle beds composed of particles of various sizes. For large-sized particles or beds with high porosity, it is speculated that countercurrent flow limitation for the two-phase fluid mixture may be the dominant mechanism that controls the quenching process, similar to the flow limitation that leads to particle bed dryout. For small-sized particles, or a mixture of particle sizes, surface tension may contribute significantly to the retardation of water flow into the dry bed.

The TMI-2 particle bed in the core consists of particles similar in size to those used in the Sandia DCC-2 experiment. The average quench heat flux of the DCC-2 particle bed was determined to be less than 20% of the dryout heat flux.[21] The quench experiment was performed from high temperatures after dryout with the internal heat generation removed. For the TMI-2 particle bed, the dryout occurred as a result of water boil-off in the core. (If water was present in the core and covered the particle bed, according to the calculation of dryout heat flux given in the last section, the particle bed would not have dried out.) When water was reintroduced into the core, the TMI-2 upper-core particle bed, unlike the one in the DCC-2 experiment, was still generating heat and could give rise to a surface heat flux more than one-third of the dryout heat flux if all the generated heat was transferred upwards. If the DCC-2 analogy is carried to the TMI-2 particle bed, it would not have been quenched for many hours after the initiation of the accident. (After three hours, it takes 20 more hours for the decay heat to drop by a factor of two.) Examination of the debris particles, however, showed that a large fraction of the material may not have exceeded 2000 K for significant lengths of time,[31] so the particle bed must have been quenched shortly after the core was covered with emergency core cooling water at around 210 min.

The apparent contradiction between the Sandia experiments and the lack of extreme heating of the TMI-2 particle bed may be due to its relatively high porosity (0.54 vs. 0.41) which reduced the effect of surface tension and led to an early quench. However, without an adequate theory that identifies the controlling mechanisms of quenching, we shall assume that the TMI-2 particle bed behaved like the ones in the experiments of

Ginsberg, et al.,[33-35] and of Cho, Armstrong, and Chan,[36] and analyze its quenching behavior accordingly, i.e., when water was introduced into the core, the heat flux at the top of the particle bed became equal to the dryout heat flux until the bed was completely quenched.

3.2 TMI-2 Upper-Core Particle Bed Quench Time Estimate

As shown by the experiments of Ginsberg, et al.,[33-35] and of Cho, Armstrong, and Chan,[36] the quench of large-sized particle beds is a two-step process. A column of liquid first moves down the particle bed in the central region, quenching the particles along its path and leaving the particles around it dry. When the liquid column reaches the bottom of the debris bed, it spreads out to peripheral areas where the remaining dry particles are quenched from the bottom up. The experiments were small-scaled, about 0.1 m in bed diameter. The TMI-2 upper-core particle bed, on the other hand, is about 2.8 m in diameter. It is conceivable that during its quench, there were many columns of water coming down during the downward quench, leaving pockets of dry particles which were later quenched from the bottom up. The experiments showed that, during the entire quench, the heat flux was approximately constant and equal to the dryout heat flux. Therefore, to estimate the quench time, it is not necessary to know the quench pattern. We assume that the quench is one-dimensional and progresses uniformly downward.

Fig. 8 illustrates the geometry and parameters involved in the quench calculation. The particle bed is of height L and the quench front along a vertical axis is denoted by z whose origin is placed at the bottom of the particle bed (or equivalently, the top of the consolidated region). The heat flux going into the particle bed from the consolidated region is denoted by q_o''. At the quench front in the particle bed, the heat flux is equal to the dryout heat flux, q_d'', for the bed. The difference between q_d'' and q_o'' is made up by the quenching of the hot particles as the quench front propagates downwards and the heat generated in the particle bed below the quench front. The equation for the propagation of the quench front is given by

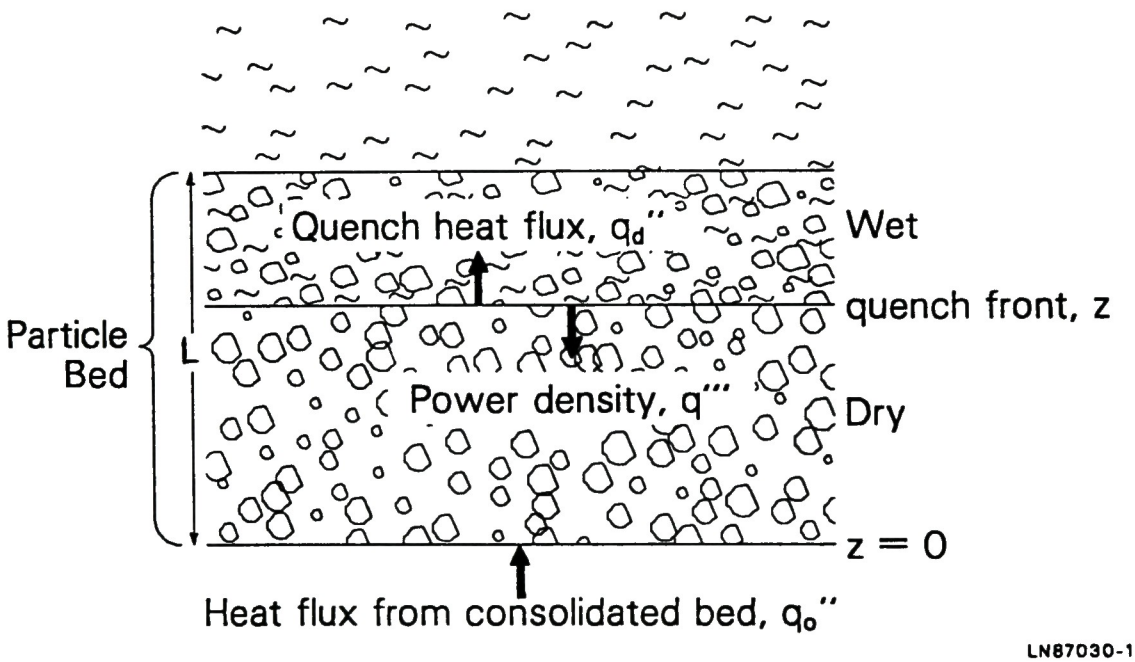

Figure 8. Illustration of the particle bed quenching process.

$$-\rho C_p (1 - c) \Delta T \frac{dz}{dt} = q_d'' - q_o'' - q''' z \quad , \tag{3-1}$$

where

ρ = material density of the particles

C_p = specific heat of the particles

c = bed porosity

ΔT = T(particle) - T(saturation) (initial temperature of particles over saturation temperature of water)

q''' = bed power density,

and the other parameters are described in the text above the equation.

The solution of Eq. (3-1) is given by

$$z = \frac{q_d'' - q_o''}{q'''} \left[1 - \left(1 - \frac{L q'''}{q_d'' - q_o''} \right) e^{t/\tau} \right] \quad , \tag{3-2}$$

where the time t is measured from the time when the bed starts to quench ($z = L$) and the time constant τ is given by

$$\tau = \rho C_p (1 - c) \Delta T / q''' \quad . \tag{3-3}$$

Substituting $z = 0$ in Eq. (3-2), we obtain the quench time, t_o, for the particle bed as

$$t_o = -\tau \log_e \left(1 - \frac{L q'''}{q_d'' - q_o''} \right) \quad . \tag{3-4}$$

The following parameters are used to estimate the quench time as given by Eq. (3-4):

ρ = 9000 kg/m^3,

C_p = 330 J/kg-K

ε = 0.54,

ΔT = 1400 K (initial temperature at 2000 K quenched to 600 K),

q''' = 0.70 MW/m^3,

τ = 2730 s,

L = 0.93 m,

q_d'' = 2.0 MW/m^2.

If 80% of the decay heat generated in the consolidated region was transferred to the particle bed (q_o'' = 1.1 MW/m^2 before relocation and q_o'' = 0.57 MW/m^2 after relocation), the time required to quench the particle bed was 3500 s (58 min) with no relocation, and 1700 s (28 min) with relocation. If no heat was transferred to the particle bed from the consolidated region, the quench time was 1100 s (18 min). Thus, the earliest time that the particle bed could have been quenched completely was 18 min after the core was covered with emergency core cooling water.

4. THERMAL HISTORY OF THE TMI-2 UPPER-CORE PARTICLE BED

In the previous sections we have examined the dryout of heat-generating particle beds and estimated the time required to quench a particle bed from high temperatures. Based on these results, in this section we attempt to construct, at least qualitatively, a thermal history of the TMI-2 particle bed in the core region from the time of its formation to the time of its final quench. Such a history is essential in the development of a detailed and consistent scenario of core damage progression. Uncertainties in the scenario will be discussed in the next section.

The particle bed in the TMI-2 core is composed mostly of shattered fuel pellets and oxidized cladding and no evidence of bulk melting occurred in the particle bed.[31] The particle bed was most likely formed when the 2-B reactor coolant pump was turned on at 174 min into the accident. By this time, the upper part of the core would have gone through a phase of rapid oxidation of the zircaloy cladding that resulted in melting the remaining zircaloy (melting point 2100 K). The molten zircaloy dissolved a small fraction of the fuel and flowed to the lower part of the core. The material that flowed down first would have solidified where it was cool enough, forming the bottom and the periphery of the consolidated region. The material that flowed down later would have rested on top of the crust, and remained molten between the fuel rods. Once the intense heat generation from rapid oxidation of the cladding ceased, the core would continue to heat up by decay heat, but at a much slower rate. Therefore, for some time the fuel rods in the central region of the core would have been standing in a molten pool of mostly zircaloy, supporting the fuel-rod remnants on top. Any fuel melting in the pool (temperature over 2800 K if eutectic formation of U-Zr-O is assumed) would have been accompanied by slumping of the fuel-rod remnants. The very presence of a particle bed in the top region of the core (which showed no evidence of bulk melting) indicates that the slumping process was incomplete when the coolant pump was turned on at 174 min. When water was delivered to the core by the pump, the peripheral assemblies, which had suffered little damage, were quenched. The steam produced from the quenching of the peripheral

assemblies could have cooled the top layer of the zircaloy-rich molten pool with embedded fuel rods and formed the top crust of the consolidated region. The fuel-rod remnants above the crust would have shattered from the sudden cooling, or simply from the pressure wave caused by the rapid steam generation, to form the particle bed.

During the pump transient, some water may have flowed into the fuel-rod remnants in the upper region of the core before they shattered to form the particle bed. The particle bed, however, could not have remained wet for very long. Steam generation from quenching a large portion of the bed and from decay heat would have driven out the water that flowed into the bed. This can be seen from comparing the dryout heat flux of the particle bed with the heat flux from quenching the particles and from decay heat. Figure 7 shows that at around 175 min, the dryout heat flux was 1.8 MW/m^2. Figure 7 also shows that the heat flux at the top of the particle bed was 0.7 MW/m^2 if all the decay power in the particle bed was transferred upwards. Quenching of a layer of the particle bed less than 0.04 m thick in one minute would have provided the additional 1.1 MW/m^2 heat flux to dry out the particle bed. After dryout, the particle bed may have been quenched slowly from the top. But before the quench front could propagate very far, the core was again uncovered due to the limited amount of water delivered by the pump, as evidenced by the reheat of the thermocouples in the peripheral assemblies a few minutes later. Therefore, between the pump transient at 174 min and emergency core coolant injection at 200 min, the particle bed may have experienced just a temporary and partial cooldown and then a reheat from decay heat.

Seven min after the initiation of emergency core coolant injection at 200 min, there would have been enough water to fill the reactor vessel, at least up to the level of the inlet and outlet nozzles of the vessel. The peripheral assemblies were again quenched, as indicated by the thermocouples in these assemblies. Because emergency core coolant injection was essentially continuous after this time (unlike the period after the pump transient), water may have covered the core for the rest of the accident. Based on the curves shown in Fig. 7, before fuel relocation to the lower plenum around 225 min, depending on the amount of heat

transferred to the particle bed from the consolidated region, the particle bed may be coolable, or only marginally coolable. If 80% of the decay heat generated in the consolidated region was transferred to the particle bed, the bed would have remained unquenched, or quenched very slowly (58 min required for complete quench); if no heat was transferred from the consolidated region to the particle bed, it would take about 18 min to completely quench the particle bed (see Section 3.2). In the first case, the bottom of the particle bed would have remained dry at the time of fuel relocation to the lower plenum from the consolidated region. In the second case, the particle bed would have been just about completely quenched by this time, or at least the bottom of the particle bed would have been covered with water, recalling that the final quench of a particle bed is from bottom up.[33-36]

With fuel relocation from the consolidated region, the decay heat from that region was accordingly reduced. Now, even if most of the decay heat generated in the consolidated region was transferred to the particle bed, the time required to quench the particle bed would have been reduced from 58 min to 28 min. If quench was initiated at 207 min, one third of the particle bed would have been quenched before relocation; after relocation, the additional time required to quench the remaining two-thirds would have been about 20 min. Therefore, at the latest, the particle bed would have been quenched by 245 min after the start of the accident. As indicated earlier, if little heat was transferred from the consolidated region to the particle bed, the particle bed could have been quenched as early as 225 min.

With continuous coolant flow through the core, the temperature in the particle bed would have stayed at or below the saturation temperature of the water after the bed was completely quenched.

5. DISCUSSION AND CONCLUSIONS

In constructing the thermal history of the TMI-2 upper-core particle bed, two aspects of particle bed heat transfer are involved. One is the dryout of particle beds immersed in water when the power in the particle bed is increased beyond a certain level such that the steam generated in the bed completely drives out the water in the bed. The other aspect is the quenching of dry particle beds from high temperatures. The understanding of these aspects, and the validity of their application to the construction of the thermal history of the TMI-2 upper-core particle bed will be discussed in this section. Conclusions regarding the thermal history of the TMI-2 particle bed during the course of the accident are drawn from these discussions.

Extensive work, both theoretical and experimental, has been done on the dryout of heat-generating particle beds. In Section 2, we have presented two models derived from apparently unrelated principles that predict the dryout heat flux of deep particle beds. One model is based on separated flow of steam and water in the particle bed. Pressure equilibrium between the phases and mass conservation are assumed. The maximum heat flux obtainable at the top of the particle bed under these constraints is identified as the dryout heat flux. The other model is based on an empirical flooding correlation for countercurrent flows of gas and liquid through a particle bed. In downward liquid and upward gas flows, if either the liquid or the gas flow is increased beyond a certain limit (termed the flooding point) the liquid is expelled violently out of the top of the particle bed. A series of such points defines a flooding curve. At the point of dryout of a particle bed, the downward liquid flow is assumed to balance the upward vapor flow and both flows are assumed to fall on the flooding line.

In the separated flow model, the pressure drop in a particle bed is based on an empirical correlation for single phase flow (the Ergun equation), but modified for each phase with a multiplier which is a function of the liquid fraction in the bed. There is some uncertainty as to the exact form of these multiplier functions. In the flooding model,

the correlation used is obtained from experiments with hollow cylinders (Raschig rings). A free parameter (the shape factor) exists for converting these particles to equivalent spherical particles. With suitable choices for the multiplier function in the separated flow model and the free parameter in the flooding model, the dryout heat fluxes predicted by both models can be made to agree within a few percent in the laminar-to-turbulent transition flow regime, which is the regime of interest for the TMI-2 upper-core particle bed.

The ability of the models to accurately predict the dryout heat flux of the TMI-2 upper-core particle bed is demonstrated by the close agreement between the predictions and the results of experiments with particle beds not too different in characteristics from the TMI-2 particle bed. If the TMI-2 upper-core particle bed was formed in cold conditions under water, uncertainties in predicting its dryout will arise, not from the prediction of the dryout heat flux, but from the amount of heat that would have been transferred to it from the consolidated region. If no heat was transferred, the heat flux through the particle bed would have been less than one half of the predicted dryout heat flux; so the particle bed never would have dried out. It is only when most of the heat generated in the consolidated region was transferred to the particle bed that dryout of the submerged particle bed was possible, because then the heat flux through the particle bed would have been comparable to the predicted dryout heat flux. However, the TMI-2 particle bed most likely was formed from dry, shattered fuel rods at high temperature. Even with no heat transfer from the consolidated region, slight quenching of the particle bed would have provided enough steam flow to drive out any water that might have entered the bed. Therefore, it seems fairly certain that the particle bed would have remained dry between the pump transient at 174 min and refill of the core with emergency core cooling water at 207 min.

The theory of the quenching of particle beds is not highly developed. It it unclear what are the basic mechanisms that control the quenching process. Experimental work on quenching is also sparse. Moreover, no experimental work has been done with the quenching of heat-generating particle beds. The particle beds in all the experiments were preheated to

high temperatures and the power in the particle beds was removed before water was poured over them. Based on the few experiments found in the literature, the evidence points to a dichotomy in the quenching behavior of particle beds. For uniform particles on the order of a few millimeters, the quenching of the bed is nonuniform. Water may drain into the bed at selected sites, leaving the remainder of the bed dry until the bed is filled from the bottom up.[33-36] The heat flux during the quenching process, however, appears constant and is approximately equal to the dryout heat flux for these beds. On the other hand, for particle beds composed of smaller particles, or a spectrum of particle sizes, the quenching heat flux appears to be several times smaller than the dryout heat flux.[21,37,38]

If the quench heat flux is comparable to the dryout heat flux, the analysis in Section 4 shows that the TMI-2 upper-core particle bed would have been quenched, at the latest, by 245 min after the start of the accident. If the quench heat flux is several times smaller than the dryout heat flux, the bed would have remained dry for many more hours, continued to heat up under decay heat, and eventually melted, regardless of any water present in the core. The fact that the particle bed never melted indicates that the particle bed was quenched, or cooled very efficiently, after emergency core coolant injection.

Based on the above discussions, we conclude by giving a brief summary of a most likely thermal history of the TMI-2 upper-core particle bed:

1. The particle bed was formed at 174 min from high temperatures when the 2-B primary coolant pump was turned on. It may have been cooled somewhat, but not quenched to the saturation temperature of the water.

2. Between 174 min and 207 min, the particle bed remained dry and recovered from the cooling during the pump transient. It rested on the top crust of the consolidated region, also formed during the pump transient, and insulated the consolidated region from coming into contact with cooling water and from radiating directly to cool structures.

3. The particle bed started to quench once it was covered with water, at about 207 min. At the time of relocation of molten material from the consolidated region to the lower plenum (225 min), the particle bed may be only partially quenched, but at least the bottom of the bed would have been covered with water.

4. After 225 min, quenching of the particle bed accelerated if not already completed and, by 245 min at the latest, the particle bed was completely quenched to the saturation temperature of the water. Thereafter, the particle bed remained immersed in water for the rest of the accident.

6. REFERENCES

1. E. L. Tolman, et al., TMI-2 Accident Scenario Update, EGG-TMI-7489, December 1986.

2. P. Kuan, TMI-2 Core Debris Bed Coolability, EGG-TMI-7150, March 1986.

3. P. Kuan, Core Relocation in the TMI-2 Accident, EGG-TMI-7402, November 1986.

4. R. J. Lipinski, "A Particle Bed Dryout Model with Upward and Downward Boiling," Trans. Amer. Nucl. Soc., 35, 358, November 1980.

5. R. J. Lipinski, A Model for Boiling and Dryout in Particle Beds, NUREG/CR-2646, SAND82-0765, June 1982.

6. A. M. White, "Pressure Drop and Loading Velocities in Packed Towers," Trans. Amer. Inst. Chem. Eng., 31, 390, June 1935.

7. E. S. Sowa, J. C. Hesson, R. H. Gebner, and G. T. Goldfuss, "Heat Transfer Experiments through Beds of UO_2 in Boiling Sodium," Trans. Amer. Nucl. Soc., 14, 2, November 1971, p. 725.

8. R. B. Bird, W. E. Stewart, and E. N. Lightfoot, Transport Phenomena, 6.4, John Wiley & Sons, New York (1960).

9. A. W. Reed, The Effect of Channeling on the Dryout of Heated Particulate Beds Immersed in a Liquid Pool, PhD Thesis, Massachusetts Institute of Technology, Cambridge, MA, February 1982.

10. R. J. Lipinski, "A Coolability Meld for Post-accident Nuclear Reactor Debris," Nucl. Technol., 65, 53, April 1984.

11. T. Schulenberg and U. Müller, as quoted by Reference 12.

12. G. Hofmann, "Dryout in Very Deep Particulate Beds," Nucl. Eng. Design, 99, 177, 1987.

13. S. Ergun, "Fluid Flow through Packed Columns," Chem. Eng. Prog., 48, 89, 1952.

14. T. K. Sherwood, G. H. Shipley, and F. A. L. Holloway, "Flooding Velocities in Packed Columns," Ind. Eng. Chem., 30, 769, 1938.

15. T. G. Theofanous and M. Saito, An Assessment of Class 9 (Core-Melt) Accidents for PWR Dry-Containment Systems, PNE-81-148, Purdue University, West Lafayette, Indiana, June 1981.

16. G. B. Wallis, One-Dimensional Two-Phase Flow, McGraw-Hill, New York (1960), p. 338.

17. G. B. Wallis, One-Dimensional Two-Phase Flow, McGraw-Hill, New York (1960), pp. 139-141.

18. R. W. Ostensen and R. J. Lipinski, "A Particle Bed Dryout Model Based on Flooding," Nucl. Sci. Eng., 79, 110, September 1981.

19. S. Uchida and S. Fujita, J. Soc., Chem. Ind. (Japan), 39, 886, 1936.

20. W. E. Lobo, L. Friend, F. Hashmall, and F. Zenz, "Limiting Capacity of Dumped Tower Packings," Trans. Amer. Inst. Chem. Engrs., 41, 693, 1945.

21. A. W. Reed, et al., DCC-1/DCC-2 Degraded Core Coolability Analysis, NUREG/CR/4390, SAND-85-1967, October 1985.

22. G. F. Stevens and R. Trenberth, "Experimental Studies of Boiling Heat Transfer and Dryout in Heat Generating Particulate Beds in Water at 1 Bar," Post Accident Debris Cooling, Proc. 5th Post Acc. Heat Removal Inf. Exchange Mtg., 1982, U. Müller and C. Günther edit., Nucl. Res. Center, Karlsruhe, pp. 108-113.

23. D. Squarer, L. E. Hochreiter, and A. T. Pieczynski, "Modes of heat Removal from a Heat-Generating Debris Bed," Nucl. Technol., 65, 16, 1984.

24. L. Barleon and H. Werle, "Dependence of Debris Bed Dryout Heat Flux on Particle Diameter, "Trans. Amer. Nucl. Soc., 38, 382, 1981.

25. G. Hofmann, "Dryout in Very Deep Particulate Beds," Nucl. Eng. Design, 99, 177, 1987.

26. L. Barleon, K. Thomauske, and H. Werle, "Cooling of Debris Beds," Nucl. Technol., 65, 67, 1984.

27. V. R. Fricke, "Core Debris Bed Probing," TMI-2 Technical Planning Bulletin, TPB-84-8, December 21, 1984.

28. L. S. Beller and H. L. Brown, Design and Operation of the Core Topography Data Acquisition System for TMI-2, GEND-INF-012, May 1984.

29. E. L. Tolman, et al., TMI-2 Core Bore Acquisition Summary Report, EGG-TMI-7385, Rev. 1, February 1987.

30. R. Rainisch, "Defueling Canisters Transfer Log," TMI-2 Technical Bulletin, TB-86-12, Rev. 4, February 25, 1987.

31. D. W. Akers, et al., TMI-2 Core Debris Grab Samples--Examination and Analysis, GEND-INF-075, September 1986.

32. TMI-2 Accident Core Heat-Up Analysis, A Supplement, NSAC-25, June 1981.

33. T. Ginsberg, et al., LWR Steam Spike Phenomenology: Debris Bed Quenching Experiments, NUREG/CR-2857, June 1982.

34. T. Ginsberg, et al., "Transient Core Debris Bed Heat Removal Experiments and Analysis," Proc. Int. Mtg. on Thermal Nuclear Reactor Safety, Chicago, IL, NUREG/CP-0027, Vol. 2, February 1983.

35. T. Ginsberg, et al., "Core Debris Quenching Heat Transfer Rates under Top- and Bottom-Flooding Conditions," Proc. Int. Mtg. on LWR Severe Accident Evaluation, Vol. 2, Cambridge, MA, August 1983.

36. D. H. Cho, D. R. Armstrong II, and S. H. Chan, "On the Pattern of Water Penetration into a Hot Particle Bed," Nucl. Technol., 65, 23, April 1984.

37. L. Barleon, K. Thomauske, and H. Werle, "Extended Dryout and Rewetting of Small-Particle Core debris," Proc. 6th Inf. Exchange Mtg. on Debris Coolability, EPIR NP-4455, March 1986, p. 17-1.

38. K. R. Boldt, A. W. Reed, and T. R. Schmidt, DCC-3 Degraded Core Coolability: Experiment and Analysis, NUREG/CR-4606, SAND-86-1033, September 1986.